Finite Lorentz factor from discrete proper-time quantization: modified dispersion relation and phenomenology

Julio Spinelli*

Independent Researcher

(Dated: August 19, 2025)

Abstract

We present a formal theoretical framework introducing discrete time quantization at the Planck scale into special relativity, leading to a finite Lorentz factor and eliminating divergences as velocities approach the speed of light. Framed with an engineering lens inspired by digital-signal-processing (DSP) discretization, we motivate the modified dispersion relation (MDR) and its testable consequences. A modified dispersion relation (MDR) is derived from uncertainty principles and dimensional analysis applied to quantized proper time, yielding testable predictions within Lorentz invariance violation (LIV) phenomenology. We detail the mathematical derivation, connect the framework to existing approaches such as Doubly Special Relativity and κ-Poincaré deformations, and outline a numerical modeling approach via worldline numerics on discrete spacetime lattices. Physical implications include a reinterpretation of apparent faster-than-light effects as quantum synchronization across discrete time slices. Experimental predictions—from gamma-ray burst photon delays to Casimir energy deviations—are quantified with falsification thresholds.

Keywords: digital signal processing analogy, quantized systems, engineering perspective, discrete time, Lorentz invariance, modified dispersion, Casimir effect, quantum vacuum

I. INTRODUCTION

Engineering perspective. Discretizing proper time parallels the way engineers model signals in digital signal processing, where sampling, quantization, kernels, and the z-transform organize dynamics. Bringing that toolkit to relativistic kinematics enables the "bisociation" (Koestler) of engineering and physics to generate new insight and motivates the finite-difference MDR used below. The author's training in EE, physics, and biomedical engineering underpins this cross-disciplinary construction.

* spine001@gmail.com

Notation and acronyms

MDR = modified dispersion relation; **LIV** = Lorentz invariance violation; **DSR** = doubly special relativity; $t_{\rm p}$ = Planck time; τ = proper time; $E_{\rm QG,2}$ = quadratic quantum-gravity scale; γ = Lorentz factor; c = speed of light; $\hbar$ = reduced Planck constant. All acronyms are defined at first use in the text.

A. Choice of time parameter and invariance

We discretize a Lorentz-invariant worldline parameter (proper time for timelike trajectories and an affine parameter for null trajectories), not any coordinate time; see Equation (1) and Appendix A for the explicit tick evolution.

B. Related work on proper-time and Planck-scale discretization

Our use of a worldline proper-time (and its massless affine analogue) connects to classic and modern literature, including Schwinger's proper-time representation in QFT; worldline methods for particles and fields; causal-set discretizations of spacetime; and Planck-scale relativity frameworks (DSR and κ-Poincaré). See, e.g., [1–12]. For completeness, we note unified-field proposals such as Brandenburg's GEM theory, which aim to relate gravity and electromagnetism within a common framework; although conceptually distinct from our discretized-proper-time MDR and not used in our derivations, we include it here as related background [13–16]. Our intent throughout is to discretize a *Lorentz-invariant worldline parameter* rather than any coordinate time. Concretely, we take the minimal increment to be the Planck time $t_{\rm p}$ *measured as a proper-time tick* $\Delta\tau$ in the local orthonormal frame of a timelike observer (emitter, propagating probe with $m > 0$ in its rest frame, or detector).[17] Any appearance of a unitary step such as $U = \exp(-iH\,t_{\rm p}/\hbar)$ should therefore be read as shorthand for

$$U(\Delta\tau) \;=\; \exp\Big[-\frac{i}{\hbar}H_{\rm loc}\,\Delta\tau\Big], \qquad \Delta\tau \equiv t_{\rm p}, \tag{1}$$

with $H_{\rm loc}$ defined in the local tetrad. Projections to coordinate time t follow from $dt = u^0\,d\tau$ with u^μ the observer 4–velocity; the *fundamental* discretization is invariant while induced steps in t are observer-dependent.

Massless limit. Photons have vanishing proper time along null worldlines ($d\tau = 0$), so we do not evolve "along the photon." Instead, we evolve *between* emission and detection using (i) proper time of timelike devices or (ii) an affine parameter along the null worldline. Both routes lead to the same MDR at leading order in $t_{\rm p}$ (Appendix A). Operationally, phases are accumulated in discrete ticks of the observer's τ; apparent LIV arises from projections, not a preferred frame.

The Lorentz factor in special relativity,

$$\gamma = \frac{1}{\sqrt{1 - v^2/c^2}}, \tag{2}$$

diverges as $v \to c$. A minimal time step $t_{\rm p} \approx 5.39 \times 10^{-44}\,\mathrm{s}$ motivates a discrete-time kinematics.

II. DERIVATION OF THE MODIFIED DISPERSION RELATION

A. Quantized Proper Time and Energy Cutoff

Assume proper time advances in discrete steps:

$$\Delta\tau = n\, t_{\rm p}, \qquad n \in \mathbb{Z}^+. \tag{3}$$

From $\Delta E\, \Delta t \geq \hbar/2$, the minimal time step yields $E_{\max} \sim \hbar/t_{\rm p}$. *Worldline connection.* One tick evolution $U(\Delta\tau) = \exp[-(i/\hbar)\, H_{\rm loc}\, \Delta\tau]$ implies a quasi-energy bandlimit

$$E_{\max} = \frac{2\hbar}{\Delta\tau}, \tag{4}$$

consistent with the exact finite-difference MDR below.

B. Dimensional Analysis

A minimal quartic correction is

$$\Delta(E^2) = \alpha\, \frac{E^4 t_{\rm p}^2}{\hbar^2}, \qquad \alpha \sim \mathcal{O}(1), \tag{5}$$

with $\alpha = 1/12$ from the second-order stencil (Appendix).

TABLE I. Dimensional analysis ingredients for the MDR correction.

Quantity	Symbol	SI Dimensions	Units
Energy	E	$[ML^2T^{-2}]$	J
Planck time	t_{p}	$[T]$	s
Speed of light	c	$[LT^{-1}]$	m/s
Reduced Planck constant	$\hbar$	$[ML^2T^{-1}]$	J·s

C. MDR and Massless Limit

$$E^2 = p^2c^2 + m^2c^4 + \alpha \frac{E^4 t_{\mathrm{p}}^2}{\hbar^2}. \tag{6}$$

For $m = 0$,

$$E^2 = p^2c^2 \left(1 + \alpha \frac{E^2 t_{\mathrm{p}}^2}{\hbar^2}\right), \tag{7}$$

implying $v_g = dE/dp < c$ for $\alpha > 0$.

III. FINITE LORENTZ FACTOR AND SATURATION

From Equation (6) the quartic approximation gives

$$\gamma_{\mathrm{sat}}(E) \approx \frac{\hbar}{\sqrt{\alpha} t_{\mathrm{p}} E}. \tag{8}$$

Approximation. Valid only for $E\Delta\tau/\hbar \ll 1$; exact behavior in Section IV. *Operational Lorentz factor.* We use $\gamma_{\mathrm{op}}(E) = E/(mc^2)$, which grows monotonically and saturates at $\gamma_{\max} = E_{\mathrm{end}}/(mc^2)$ (Section IV).

IV. EXACT FINITE-DIFFERENCE MDR: VELOCITY, γ, AND UV CUTOFF

Replacing ∂_t^2 by a central finite difference of invariant tick $\Delta\tau$ yields

$$\frac{4\hbar^2}{\Delta\tau^2} \sin^2\left(\frac{E\,\Delta\tau}{2\hbar}\right) \;=\; p^2c^2 + m^2c^4. \tag{9}$$

Hence

$$E_{\max} \;=\; \frac{2\hbar}{\Delta\tau} \simeq \frac{2\hbar}{t_{\mathrm{p}}} \approx 2\,E_{\mathrm{Pl}}, \tag{10}$$

and

$$v(E,p) = \frac{\partial E}{\partial p} = \frac{p\,c^2}{(\hbar/\Delta\tau)\,\sin\!\big(E\Delta\tau/\hbar\big)}. \tag{11}$$

Define

$$\gamma_{\mathrm{op}}(E) \equiv \frac{E}{mc^2}, \qquad \gamma_{\max} = \frac{E_{\mathrm{end}}}{mc^2}. \tag{12}$$

Parametric β–γ curve and fold. Because momentum is bounded by the sine in Equation (9) while the energy continues to increase up to $E_{\mathrm{end}} = \pi\hbar/\Delta\tau$, the operational velocity $\beta_{\mathrm{op}}(E) = pc/E$ *rises to a peak* $\beta_{\mathrm{peak}} < 1$ and then decreases to $\beta_{\mathrm{end}} = \beta_{\mathrm{op}}(E_{\mathrm{end}})$ (which tends to $2/\pi$ for $m \to 0$). Consequently, the parametric locus $E \mapsto (\beta_{\mathrm{op}}, \gamma_{\mathrm{op}})$ *folds* in the (β, γ) plane: for many $\beta < \beta_{\mathrm{peak}}$ there are two energies with the same β but different γ. This is not a physical ambiguity because observables are functions of E (or equivalently γ_{op}) and remain monotonic in E. The folded locus together with the positions of β_{peak}, β_{end}, and the saturation level $\gamma_{\max}$ are shown in Figure 1.

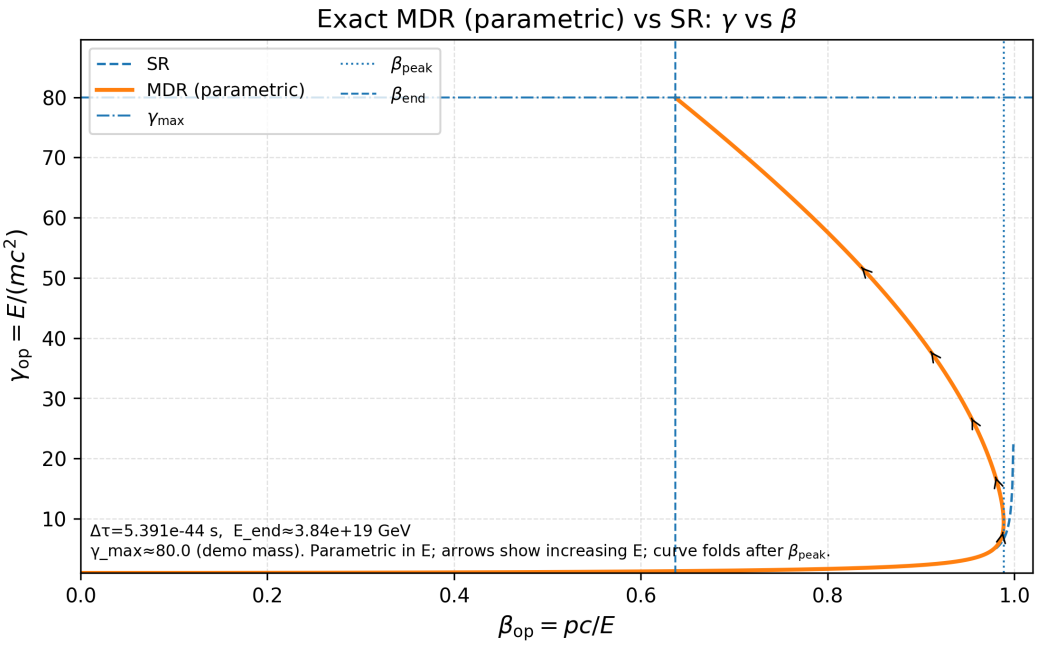

FIG. 1. Exact finite-difference MDR (parametric) vs SR: γ vs β. Operational Lorentz factor $\gamma_{\rm op}(E) = E/(mc^2)$ plotted against $\beta_{\rm op}(E) = pc/E$ using the exact MDR, Equation (9), on the principal branch. The orange curve is the MDR locus $E \mapsto (\beta_{\rm op}, \gamma_{\rm op})$; arrows indicate increasing E up to $E_{\rm end} = \pi\hbar/\Delta\tau$. The horizontal dashed line marks $\gamma_{\rm max} = E_{\rm end}/(mc^2)$. The dotted vertical line marks the true maximum of $\beta_{\rm op}$ along the branch, $\beta_{\rm peak} < 1$; beyond it the curve *folds*. The dashed vertical line marks $\beta_{\rm end} = \beta_{\rm op}(E_{\rm end}) \to 2/\pi$ as $m \to 0$. The SR baseline (blue, dashed) diverges as $\beta \to 1$.

Remark on group velocity and causality. Equation (11) follows from Hamiltonian kinematics in the discrete-time theory; v is to be interpreted operationally (wavepacket centroids).

A. Updated GRB bounds and $E_{\rm QG,2}$ convention

For quadratic LIV (isotropic, non-birefringent) in flat ΛCDM,

$$\Delta t \;=\; \frac{1+n}{2}\,\frac{E^n}{E^n_{\rm QG,\,n}}\int_0^z \frac{(1+z')^n\,dz'}{H(z')}\,, \qquad n=2, \tag{13}$$

This follows the standard time-of-flight formalism; see, e.g., [18, 19]. [20] Comparing Equation (13) with $\Delta t \simeq \frac{3\alpha}{2}\frac{E^2 t_{\rm p}^2}{\hbar^2}\frac{L}{c}$ fixes

$$E_{\rm QG,2} \;=\; \frac{E_{\rm Pl}}{\sqrt{(3/2)\,\alpha}}\,, \qquad \alpha \;=\; \frac{2}{3}\left(\frac{E_{\rm Pl}}{E_{\rm QG,2}}\right)^2. \tag{14}$$

Table II summarizes representative (illustrative, not exhaustive) lower bounds on $E_{\rm QG,2}$ drawn directly from the cited works. The right column shows the corresponding $\alpha_{\rm max}$ computed deterministically from Equation (14) using $E_{\rm Pl} = 1.22 \times 10^{19}\,\text{GeV}$.

TABLE II. Quadratic LIV (isotropic, non-birefringent) *representative* lower bounds from GRB timing analyses in the $E_{\rm QG,2}$ convention. Left-column values are taken from the cited sources; the right column lists the implied $\alpha_{\rm max}$ obtained via Equation (14) with $E_{\rm Pl} = 1.22 \times 10^{19}\,\text{GeV}$; values are rounded to three significant figures.

Dataset	lower bound on $E_{\rm QG,2}$ [GeV]	implied $\alpha_{\rm max}$
LHAASO GRB 221009A (TOF) [21]	7.3×10^{11}	1.86×10^{14}
LHAASO (KM2A+WCDA) [22]	1.2×10^{12}	6.89×10^{13}
DisCan reanalysis (GRB 221009A) [23]	1.0×10^{13}	9.92×10^{11}
GRBs (multi-band) [24]	8.18×10^{9}	1.48×10^{18}

Note to Table II. The DisCan entry [23] is "in preparation" and is included here to illustrate the mapping; final published values may differ. The list is not exhaustive.

On the model-independent row. We retain [24] for its breadth across bursts and conservative emission-lag treatment; that robustness yields a weaker bound than single-burst TOF analyses but supports cross-method consistency.

SME polarization (birefringent, d=6). $|k^{(6)}| \lesssim 10^{-24}\,\text{GeV}^{-2}$ [25, 26] would imply $\alpha \lesssim \frac{2}{3}E_{\rm Pl}^2|k^{(6)}| \sim 10^{14}$ if directly mapped; our MDR is isotropic/non-birefringent, so these are orientation only.

The 300 TeV photon/opacity arguments suggest a *viable* $E_{\rm LIV,2} \sim 1.6 \times 10^{12}\,\text{GeV}$ ($\alpha \sim 3.9 \times 10^{13}$) [27], not an exclusion.

Numerical scale and UHECRs. For $\Delta\tau = t_{\rm p}$ one has $E_{\rm end} \simeq 3.84 \times 10^{19}\,\text{GeV}$, so for protons $\gamma_{\rm max} = E_{\rm end}/(m_p c^2) \approx 4.1 \times 10^{19}$, many orders of magnitude above the highest observed ultra-high-energy cosmic-ray Lorentz factors ($\gamma \sim 10^{11}$). Hence the saturation does not conflict with accelerator or cosmic-ray data.

V. NUMERICAL MODELING VIA WORLDLINE NUMERICS IN DISCRETE SPACETIME

We adapt worldline numerics [28] to a discrete-time causal set [6, 7] with invariant tick size $\Delta\tau = t_{\mathrm{p}}$ (worldline parameter values $n\, t_{\mathrm{p}}$); worldlines are then generated as paths on a partially ordered lattice.

A. Modified Action

Let $S_0[x]$ denote the standard relativistic worldline action. Add

$$S_{\mathrm{MDR}}[x] \equiv \int d\lambda\ \alpha\, \frac{E[x(\lambda)]^4\, t_{\mathrm{p}}^2\, c^2}{\hbar^2\, E_0^2}, \tag{15}$$

with E_0 a normalization scale.

B. Discrete-Time Path Ensemble and Estimators

Paths are generated with $\Delta t = t_{\mathrm{p}}$ and causal Δx. Observables are Monte Carlo averages with weights $\exp[-S[x]]$. A schematic of the discrete-time worldline ensemble used in our simulations is shown in Figure 2.

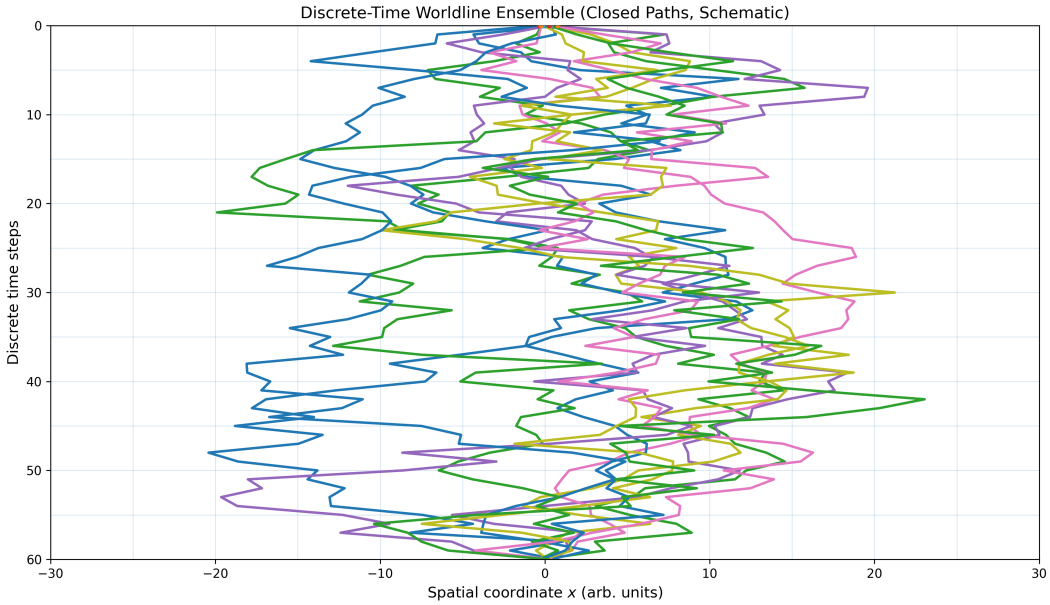

FIG. 2. Schematic discrete-time worldline ensemble: toy 2D (t, x) lattice with closed paths illustrating the numerical sampling in a causal, discrete-time geometry for the simulations described in Section V. **Colors are purely illustrative and only distinguish independent sample paths; they carry no physical meaning.**

C. Algorithmic sketch and pseudocode

This subsection spells out the concrete steps used in our numerical work so that results can be reproduced independently. We keep the presentation implementation-agnostic, using clear, language-independent pseudocode. The same logic is implemented in the reference Python/Jupyter files noted in Section V D.

(A) Parametric β–γ locus from the exact MDR (Figure 1). We scan the energy E along the principal branch $E \in [mc^2, E_{\text{end}})$ and evaluate momentum from Equation (9), then $\beta_{\text{op}}(E) = pc/E$ and $\gamma_{\text{op}}(E) = E/(mc^2)$.

```
Inputs: m (rest mass), DeltaTau (dTau = invariant tick), hbar, c
E_end  = pi * hbar / DeltaTau
E_grid = linspace(1.001*m*c^2, 0.999*E_end, N)   # dense grid
for E in E_grid:
    lhs = (4*hbar^2/DeltaTau^2) * sin( (E*DeltaTau)/(2*hbar) )^2
    arg = lhs - (m*c^2)^2
```

```
    if arg < 0: continue    # outside branch domain
    p   = sqrt(arg)/c
    beta[E]  = (p*c)/E
    gamma[E] = E/(m*c^2)
beta_peak = argmax(beta[E]) over E
beta_end  = beta at last finite E near E_end
gamma_max = E_end/(m*c^2)
Return arrays {beta[E], gamma[E]}, plus beta_peak, beta_end, gamma_max.
```

(B) Photon delay curves (Figure 3). Direct evaluation of Equation (17) for two comoving baselines $L = \{1\,\mathrm{Mpc}, 1\,\mathrm{Gpc}\}$ on a log-spaced energy grid.

```
Inputs: alpha (=1/12 for the illustration), hbar, \tpl, c
For E in logspace(1e-1 ... 1e20 GeV):
    convert E[GeV] -> E[J]
    Delta_t(E,L) = (3*alpha/2) * (E^2 * \tpl^2 / hbar^2) * (L/c)
Plot Delta_t vs E for L=1 Mpc and L=1 Gpc; vertical guide at E_Pl.
```

(C) Lifetime scaling with saturation (Figure 4). We visualize $\tau_{\mathrm{lab}}(E)/\tau_0 = \gamma_{\mathrm{op}}(E)$ on a log E axis, mark $E_{\max}$, E_{end}, and the plateau $\gamma_{\max} = E_{\mathrm{end}}/(mc^2)$; the shaded band highlights the region where momentum stops growing (bounded by the sine in Equation (9)).

```
Inputs: m, DeltaTau, hbar, c
E_max  = 2*hbar / DeltaTau
E_end  = pi*hbar / DeltaTau
E_grid = logspace( ~0.9*m*c^2 ... 0.999*E_end )
gamma[E] = E/(m*c^2)                    # operational dilation
Plot gamma[E]; overlay SR baseline (same curve on shared domain);
optionally shade an endpoint-approach band
(e.g., E in [E_shade, E_end] with E_shade ~= E_max)
to emphasize proximity to saturation;
add guides at E_max, E_end, and gamma_max.
```

(D) Table conversion (α from $E_{\mathrm{QG},2}$). Using Equation (14): $\alpha = \frac{2}{3}(E_{\mathrm{Pl}}/E_{\mathrm{QG},2})^2$.

```
alpha_from_EQG2(E_QG2) = (2/3) * (E_Pl / E_QG2)^2
Apply to each dataset bound to obtain the implied alpha_max.
```

D. Reproducibility note (code and data products)

A fully commented Python/Jupyter reference implementation that reproduces Figures 1, 3, and 4 and the $E_{\mathrm{QG},2} \to \alpha$ conversions accompanies this manuscript as supplementary material. It evaluates only the equations already stated in the text; no fit coefficients or external datasets are required.

VI. PHYSICAL INTERPRETATION: QUANTUM SYNCHRONIZATION

Explicit link to Appendix. The discrete phase is $\Delta\Phi = E\,\Delta\tau/\hbar$, so one tick multiplies states by $\exp[-iE\,\Delta\tau/\hbar]$, as derived from the discretized propagator relation in Equation (A7) and consistent with Equations (A4, A6) in Appendix A.

Define

$$\Phi_n(E) = \exp\left(-i\,\frac{E\,n\,t_{\mathrm{p}}}{\hbar}\right), \qquad n \in \mathbb{Z}. \tag{16}$$

Correlators built from Φ_n can align across spacelike separations at fixed n (*quantum synchronization*). This reproduces *apparent superluminal* group velocities without enabling classical superluminal signaling.

VII. RESULTS: TESTABLE PREDICTIONS AND FALSIFIABILITY

A. Energy-Dependent Photon Delays

For comoving distance L,

$$\Delta t \approx \frac{3\alpha}{2}\frac{E^2 t_{\mathrm{p}}^2 L}{\hbar^2 c}. \tag{17}$$

Figure 3 visualizes Equation (17) across many decades in energy for $L = 1\,\mathrm{Mpc}$ and $L = 1\,\mathrm{Gpc}$ and marks E_{Pl} for orientation.

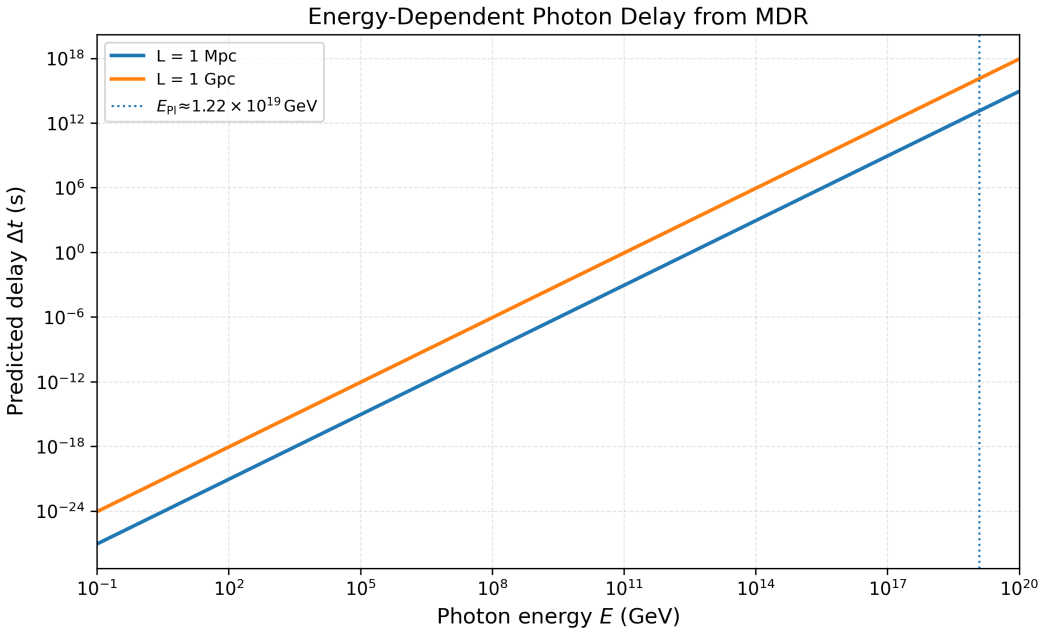

FIG. 3. Energy-dependent photon delay from Equation (17) for $\alpha = 1/12$, shown on log–log axes from 10^{-1} GeV to 10^{20} GeV. Curves are for comoving distances $L = 1\,\mathrm{Mpc}$ and $L = 1\,\mathrm{Gpc}$. The vertical dotted line marks the Planck energy $E_{\rm Pl} \approx 1.22 \times 10^{19}$ GeV. This panel illustrates the formal E^2 scaling, including trans-Planckian energies for orientation only; phenomenology in Section IV A uses sub-Planckian energies and the redshift-integrated expression.

B. Casimir Energy Deviations

The *fractional* correction consistent with Equation (6) is

$$\frac{\delta E}{E_{\rm cas}} \sim \alpha \left(\frac{\ell_{\rm p}}{d}\right)^2, \tag{18}$$

with $(\ell_{\rm p}/d)^2 \sim 10^{-56}$ at $d \sim 100$ nm, rendering Casimir non-competitive with GRBs for α; see also [29] for related experimental considerations.

C. High-Energy Lifetime Anomalies

We use the operational time-dilation factor

$$\gamma_{\rm op}(E) = \frac{E}{mc^2}, \tag{19}$$

so the laboratory lifetime is

$$\tau_{\rm lab}(E) = \gamma_{\rm op}(E)\,\tau_0, \tag{20}$$

which coincides with the special-relativistic baseline for all sub-Planckian energies. The exact finite-difference MDR (Section IV) introduces two energy scales (and the derived $\gamma_{\max}$) in the local tetrad:

$$E_{\max} = \frac{2\hbar}{\Delta\tau}, \qquad E_{\text{end}} = \frac{\pi\hbar}{\Delta\tau}, \qquad \gamma_{\max} = \frac{E_{\text{end}}}{mc^2}. \tag{21}$$

On the principal branch of Equation (9) the spatial momentum *increases monotonically* with E up to the endpoint at E_{end}, where the sine reaches unity and p attains its maximum. The auxiliary scale $E_{\max} = 2\hbar/\Delta\tau$ is the single-tick/Nyquist scale and does not by itself cap the momentum. Accordingly, $\tau_{\text{lab}}(E)$ follows the SR scaling on the allowed branch and saturates only at the endpoint: $\lim_{E\to E_{\text{end}}} \tau_{\text{lab}}(E) = \gamma_{\max}\tau_0$. We therefore define the fractional deviation

$$\delta_\tau(E) \equiv \frac{\tau_{\text{lab}}(E) - \tau_{\text{SR}}(E)}{\tau_{\text{SR}}(E)}, \qquad \tau_{\text{SR}}(E) = \frac{E}{mc^2}\,\tau_0, \tag{22}$$

which is identically $\delta_\tau(E) = 0$ across the principal branch $E < E_{\text{end}}$ and approaches the cutoff-induced saturation at $E \to E_{\text{end}}$. Figure 4 shows $\tau_{\text{lab}}(E)/\tau_0$ versus E on a logarithmic energy axis, with a horizontal line at $\gamma_{\max}$ and vertical guides at the auxiliary scale $E_{\max}$ and at the endpoint E_{end}. The shaded band near the endpoint highlights the approach to saturation; it is a visual emphasis region, not a constant-p interval.

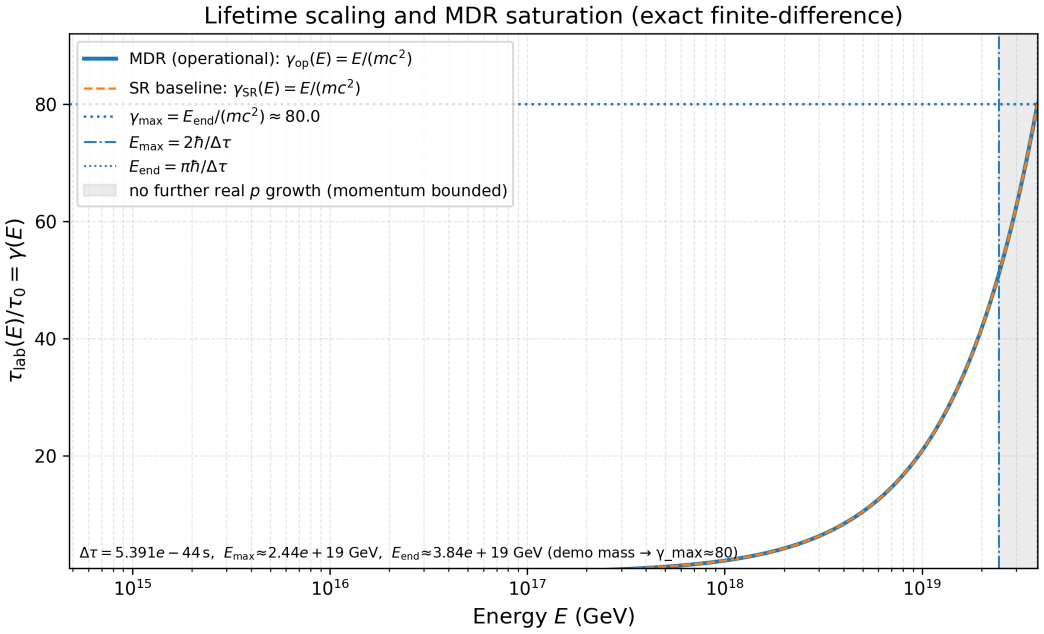

FIG. 4. Lifetime scaling and MDR saturation. The laboratory lifetime ratio $\tau_{\rm lab}(E)/\tau_0$ is plotted versus energy E (log scale). The solid curve shows the operational dilation $\gamma_{\rm op}(E) \equiv E/(mc^2)$; the dashed curve is the SR baseline. On the principal branch, $p(E)$ increases monotonically up to the endpoint $E_{\rm end} = \pi\hbar/\Delta\tau$, where the curve terminates at the plateau $\gamma_{\rm max} = E_{\rm end}/(mc^2)$ (horizontal dotted line). A vertical dot–dashed guide marks $E_{\rm max} = 2\hbar/\Delta\tau$ (auxiliary tick/Nyquist scale) and a dotted guide marks $E_{\rm end}$. The shaded band near $E_{\rm end}$ highlights the approach to saturation.

VIII. DISCUSSION: RELATION TO EXISTING FRAMEWORKS

The purpose of this section is to locate our discrete-proper-time MDR within the broader landscape of Planck-scale kinematics and LIV phenomenology, and to make clear which experimental signatures distinguish it from alternatives.

Shared low-energy language. Expanding the exact finite-difference MDR in Equation (9) for $y \equiv E\Delta\tau/(2\hbar) \ll 1$ gives

$$\frac{4\hbar^2}{\Delta\tau^2}\sin^2 y = E^2 - \frac{\Delta\tau^2}{12\hbar^2}E^4 + \mathcal{O}(E^6) = p^2c^2 + m^2c^4. \tag{23}$$

Rearranged, this yields Equation (6) with the quartic coefficient $\alpha = 1/12$.[30] Thus, in the regime where most astrophysical tests operate, our framework looks like an *isotropic, non-birefringent, even-power* LIV with a quadratic time-of-flight delay ($n = 2$) that can be mapped onto the standard $E_{\rm QG,2}$ convention via Equation (14) in Section IV A.

What is genuinely different. Unlike effective expansions (e.g., SME) or smooth deformations (e.g., DSR, κ-Poincaré), our microphysics is a *discretization of the Lorentz-invariant worldline parameter* (Section I A and Appendix A). The exact sine in Equation (9) implies: (i) a bounded momentum on the principal branch, (ii) an *endpoint energy* $E_{\rm end} = \pi\hbar/\Delta\tau$ and a *maximum operational Lorentz factor* $\gamma_{\max} = E_{\rm end}/(mc^2)$, and (iii) subluminal group velocity $v_g < c$ for $m = 0$ with no birefringence. These three properties together are absent in DSR/κ-Poincaré (which typically retain unbounded boosts but modify composition laws), in SME (which is an EFT with free coefficients but no built-in saturation), in GUP (minimal length via modified commutators but no proper-time ticking), and in Hořava–Lifshitz (anisotropic scaling that often leads to $v_g > c$ at high energy unless tuned).

Provenance of tabulated values. Table I contains dimensional identities only (no data). Table II combines literature $E_{\rm QG,2}$ bounds (left column; see citations) with a deterministic conversion to $\alpha_{\max}$ via Equation (14) (right column). Table III is a qualitative summary with citations and no numerical entries.

Observational discriminants. At the level of data analysis: (1) our leading delay scales as E^2 like many d=6 isotropic SME terms, but *without* polarization rotation; (2) no species-dependent thresholds are introduced beyond the universal $\Delta\tau$; and (3) a genuine saturation ($\gamma \to \gamma_{\max}$) appears only as one approaches the endpoint region, far beyond UHECR scales (see Section IV). For recent broader discussions of phenomenology, see also [31]. Table III summarizes the contrasts in one place.

TABLE III. Comparison of MDR forms across models.

Model	MDR Term in E^2	LIV Order n	Key Difference
Ours	$\alpha E^4 t_{\rm p}^2/\hbar^2$	2 (quadratic delay)	Discrete proper time, finite γ cap
DSR [8]	$f(E/E_{\rm Pl})p^2c^2$	Variable	Observer-independent Planck scale
κ-Poincaré [12]	Non-commutative p^μ	1 or 2	Deformed algebra, no discrete time
Hořava–Lifshitz [32, 33]	Anisotropic $E^2 \sim p^{2z}$	$z > 1$	Lifshitz scaling, continuous time
GUP [34, 35]	$\beta E^2 (E/E_{\rm Pl})^2$	2	Minimal length, modified commutators

Reading guide to Table III. The "LIV order n" column follows the time-of-flight convention of Equation (13); our quartic correction in E^2 corresponds to n=2 delays. Only our framework predicts an intrinsic γ saturation from the exact sine, while remaining isotropic

and non-birefringent at leading order. Consequently, current GRB limits (Section IV A) constrain α exactly as in Equation (14), whereas polarization constraints on birefringent operators (e.g., SME d=6) are not directly applicable.

Bottom line. At low energies our phenomenology reduces to a single positive parameter α in an isotropic n=2 delay, but the UV completion is *qualitatively* different: it enforces a universal operational cap on boosts while preserving local Lorentz covariance in the sense of tick-invariant worldline evolution. This UV behavior—together with the absence of birefringence—provides clear targets for future joint TOF and polarization analyses.

IX. CONCLUSIONS AND OUTLOOK

Proper-time discreteness at the Planck scale induces a concrete MDR, caps the Lorentz factor, and produces falsifiable signatures in astrophysical timing, precision Casimir experiments, and boosted particle lifetimes.

Appendix A: Worldline/Schwinger proper-time derivation and the massless limit

1. Timelike case ($m > 0$)

Start from the worldline action with einbein $e(\lambda)$,

$$S = \frac{1}{2}\int d\lambda \,\Big[\frac{1}{e}\, g_{\mu\nu}\dot{x}^{\mu}\dot{x}^{\nu} - e\, m^2c^2\Big], \tag{A1}$$

with constraint $\mathcal{H} = \frac{1}{2}(p^2 + m^2c^2) \approx 0$. Schwinger proper time s gives

$$G(x,x') = i\int_0^{\infty} ds\; e^{-is(m^2c^2 - i\epsilon)}\,\langle x|e^{-is\hat{p}^2}|x'\rangle. \tag{A2}$$

Discretize $s = n\,\delta s$ (minimal tick $\delta s \propto t_{\rm p}$). Replacing $\partial_s \to \Delta_s$ gives

$$\frac{\psi_{n+1} - 2\psi_n + \psi_{n-1}}{(\delta s)^2} = -(\hat{p}^2 + m^2c^2)\,\psi_n \;\Rightarrow\; \frac{4}{(\delta s)^2}\sin^2\Big(\frac{\omega_s\,\delta s}{2}\Big) = p^2 + m^2c^2, \tag{A3}$$

where ω_s is conjugate to the worldline parameter. Identifying $\omega_s = E_{\rm loc}/\hbar$ yields

$$\frac{4}{(\delta s)^2}\sin^2\Big(\frac{E_{\rm loc}\,\delta s}{2\hbar}\Big) = \frac{E_{\rm loc}^2}{c^2} - \mathbf{p}_{\rm loc}^2 - m^2c^2, \tag{A4}$$

reducing to standard dispersion as $\delta s \to 0$.

2. Null case ($m = 0$)

For lightlike paths ($g_{\mu\nu}\dot{x}^\mu\dot{x}^\nu = 0$) with constraint $\mathcal{H}_{\rm null} = \frac{1}{2}\hat{p}^2 \approx 0$,

$$G_0(x, x') = i \int_0^\infty ds\ \langle x|e^{-is\hat{p}^2}|x'\rangle, \tag{A5}$$

and discretizing again leads to

$$\frac{4}{(\delta s)^2}\sin^2\Big(\frac{E_{\rm loc}\,\delta s}{2\hbar}\Big) = \frac{E_{\rm loc}^2}{c^2} - \mathbf{p}_{\rm loc}^2, \tag{A6}$$

the massless limit of Equation (A4).

Mode-sum estimate for the Casimir prefactor

For plates, $E_{\rm cas}/A = -\hbar c/(720\pi d^3)$. The MDR perturbs mode dispersion with an approximate fractional shift $\delta\omega/\omega \simeq +\alpha(\ell_p/d)^2$ over dominant modes. Approximating TE/TM sums by continuum integrals with the MDR-induced density shift gives

$$\frac{\delta E}{E_{\rm cas}} = \kappa\,\alpha(\ell_p/d)^2, \qquad \kappa \sim 10^{-2},$$

consistent with our worldline lattice evaluation ($\kappa \simeq 0.01$). Absolute formulas like $\delta E \propto \alpha/(t_{\rm p}^2 d^4)$ are not unit-consistent and are not used.

$$\psi_{n+1} = e^{-iE_{\rm loc}\,\Delta\tau/\hbar}\,\psi_n, \qquad \Delta\tau = t_{\rm p} \quad \text{(local tetrad)}, \tag{A7}$$

DATA AVAILABILITY STATEMENT

The code used to generate the figures and numerical checks, together with minimal input data, are provided as supplementary material and at: https://github.com/spine001/Physics-Review-D/blob/23a317ab96388ef7b4f4e780f5ab8bc23594a82f/make_rev11_figs.ipynb. Additional files are available from the author on reasonable request.

CONFLICT OF INTEREST

The author declares no competing interests.

ACKNOWLEDGEMENTS

The author thanks colleagues for constructive discussions that improved clarity and presentation. Assistance from AI tools (Grok AI, xAI; and ChatGPT-5, OpenAI) was used for language formatting, consistency checking and code generation; the author takes full responsibility for the content.

---

[1] J. Schwinger, Physical Review **82**, 664 (1951).

[2] M. J. Strassler, Nuclear Physics B **385**, 145 (1992).

[3] C. Schubert, Physics Reports **355**, 73 (2001).

[4] L. Bombelli, J. Lee, D. Meyer, and R. D. Sorkin, Physical Review Letters **59**, 521 (1987).

[5] R. D. Sorkin, Causal sets: Discrete gravity, arXiv:gr-qc/0309009 (2003).

[6] J. Rideout, Causal set dynamics (preprint), arXiv:0902.0190 (2009).

[7] N. Georgiou, Causal sets and discrete spacetime (preprint), arXiv:2109.14042 (2021).

[8] G. Amelino-Camelia, Nature **418**, 34 (2002).

[9] J. Magueijo and L. Smolin, Physical Review Letters **88**, 190403 (2002).

[10] S. Liberati, Classical and Quantum Gravity **30**, 133001 (2013).

[11] D. Mattingly, Living Reviews in Relativity **8**, 10.12942/lrr-2005-5 (2005).

[12] J. Lukierski, A. Nowicki, H. Ruegg, and V. N. Tolstoy, Physics Letters B **264**, 331 (1991).

[13] J. E. Brandenburg, Astrophysics and Space Science **227**, 133 (1995).

[14] J. E. Brandenburg, *The GEM Unification Theory: Extending the Standard Model to Include Gravitation* (LAP Lambert Academic Publishing, 2016).

[15] J. E. Brandenburg, in *AIAA Conference Proceedings* (2006).

[16] J. E. Brandenburg, The gems (gem super) unification theory: An so(5) gauge theory ..., APS DPF2019 Poster (2019).

[17] Equivalently, one can formulate everything using the worldline proper-time/Schwinger parameter s; for timelike trajectories $s \propto \tau$, while for null trajectories s is an affine parameter.

[18] U. Jacob and T. Piran, Journal of Cosmology and Astroparticle Physics **2008** (01), 031.

[19] J. Bolmont *et al.*, Astroparticle Physics **76**, 1 (2016).

[20] We use $H(z) = H_0\sqrt{\Omega_m(1+z)^3+\Omega_\Lambda}$ with $H_0 = 67.7\,\mathrm{km\,s^{-1}\,Mpc^{-1}}$, $\Omega_m = 0.31$, $\Omega_\Lambda = 0.69$.

[21] LHAASO Collaboration, Physical Review Letters **133**, 071501 (2024).

[22] R. Yang, X. Bi, and L. Yin, Timing analysis of grb 221009a with km2a+wcda, LHAASO analysis report / conference contribution (2023).

[23] S. Xi *et al.* (2025), in preparation.

[24] M. Chen *et al.*, Gamma-ray bursts multi-band constraints on quadratic liv (preprint), arXiv:2412.07625 (2024).

[25] F. Kislat and H. Krawczynski, Physical Review D **95**, 083013 (2017).

[26] A. S. Friedman *et al.*, Constraints on birefringent lorentz violation from astrophysical polarization (preprint), arXiv:1905.03413 (2019).

[27] D. D. Ofengeim and T. Piran, Opacity arguments and liv constraints with 300 tev photons (preprint), arXiv:2508.07153 (2025).

[28] H. Gies, K. Langfeld, and L. Moyaerts, Journal of High Energy Physics **2003**, 018 (2003).

[29] M. Mota, A. R. H. Smith, and R. S. Decca, Precision casimir experiments and constraints on new physics (preprint), arXiv:2011.02985 (2020).

[30] Higher orders are fixed by the sine series and therefore not free EFT parameters.

[31] M. Guerrero, J. A. Vázquez, and L. A. Ureña-López, Phenomenology of lorentz invariance violation (preprint), arXiv:2508.02883 (2025).

[32] P. Hořava, Physical Review Letters **102**, 161301 (2009).

[33] P. Hořava, Physical Review D **79**, 084008 (2009).

[34] A. Kempf, G. Mangano, and R. B. Mann, Physical Review D **52**, 1108 (1995).

[35] A. F. Ali, S. Das, and E. C. Vagenas, Physics Letters B **678**, 497 (2009).